

A 34fJ 10b 500 MS/s Partial-Interleaving Pipelined SAR ADC

Yan Zhu, Chi-Hang Chan, Sai-Weng Sin, Seng-Pan U¹, R.P.Martins²

State-Key Laboratory of Analog and Mixed Signal VLSI, FST, University of Macau, Macao, China

E-mail: yanjulia@ieee.org

1 - Also with Synopsys - Chipidea Microelectronics (Macao) Limited

2- On leave from Instituto Superior Técnico/TU of Lisbon, Portugal

Abstract

A 10b 500MS/s ADC is presented that shares a full-speed SAR at front-end and interleaves the pipelined residue amplification with shared opamp and 2nd-stage SAR ADCs, which achieves high speed, low power and compact area. The prototype ADC in 65nm CMOS achieves a mean SNDR of 55.4dB with 8.2mW power dissipation at 1.2V. The active die area including the offset calibrations is 0.046mm².

Introduction

Low power consumption and high speed ADCs are highly demanded for battery-powered mobile applications. For high-resolution ($\geq 10b$), pipeline [1]-[3] and time-interleaved (TI) pipelined-SAR [4] ADCs are the most potential architectures to achieve high speed ($>200MS/s$), while their FoM are $>90fJ/conv.-step$. This paper proposes a partial interleaved pipelined-SAR architecture that implements a high speed single channel SAR for front-end sampling and conversion, which is then pipelined by time interleaved 2nd-stage low speed SAR ADCs. The design eliminates the sampling mismatches from TI-scheme and achieves high resolution, high speed and low power dissipation.

ADC Architecture and Implementation

Fig. 1 shows the ADC architecture and its timing diagram. The 1st-stage implements a high-speed 6b 2b/cycle SAR ADC. By using interpolation, two pairs of differential capacitive DACs (DAC_A and DAC_B) instead of 3 are employed for the front-end sampling and conversion. Only the residue voltage at DAC_A is processed and amplified by a low inter-stage gain of 4 and pipelined to 2nd-stage SAR ADCs in a $2 \times TI$ with opamp-shared scheme. The TI residue amplification capacitor arrays (RAC_{A1} and RAC_{A2}) also serve as a reference division [5] for the 1st-stage ADC. The 2nd-stage consists of two TI-1b/cycle SAR ADCs that determine 5b output. Each SAR is built with a 6b split-DAC where extra 1 bit is for the offset cancellation [5]. Two stages have 1b overlapping for digital error correction that relaxes the conversion accuracy of 1st-stage to 7b, including the settling and matching of DAC_A and DAC_B.

During the sampling phase ($\Phi_s=1 \& \Phi_1=1$), the differential input signal $\pm V_{in}$ are sampled onto the DAC_A, DAC_B, RAC_{A1} and RAC_B, simultaneously. In the conversion phase ($\Phi_c=1 \& \Phi_1=1$) the 1st-stage solves the coarse 6b in 3 cycles (1.2ns), and the residue is generated within the DAC_A and RAC_{A1}. When the conversion is completed ($\Phi_2=1$), the RAC_{A1} disconnects to DAC_A and connects to the opamp's input. The residue at the top-plate of RAC_{A1} is amplified to 2nd-stage SAR.

This work was financially supported by University of Macau and Macao Science & Technology Development Fund (FDCT).

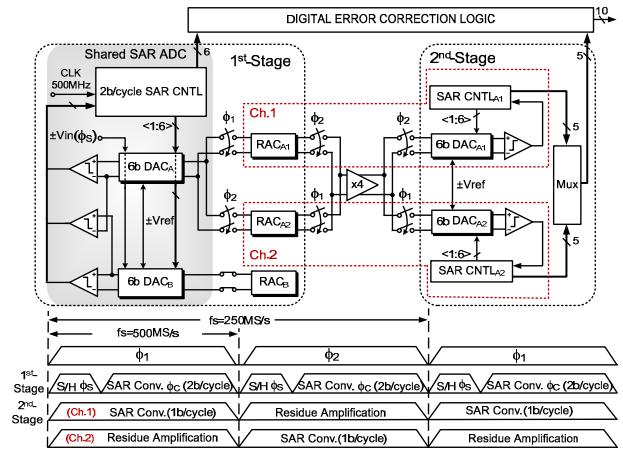


Fig. 1 Overall ADC architecture and its timing diagram.

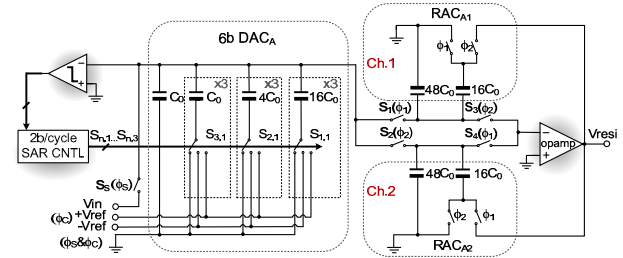


Fig. 2 1st-stage 6b SAR ADC w/ Opamp-shared TI-Residue Amplification.

Meanwhile the DAC_A switched to RAC_{A2} starts a new conversion. In the subsequent pipelined phase ($\Phi_1=1$) when the rest 5b is determined by the 2nd-stage SAR, it is passed to digital error correction logic for the final 10b output. The front-end SAR ADC operates at 500MS/s, while each interleaved channel works at 250MS/s with an equivalent duration of 2ns to perform the amplification and conversion.

Fig. 2 shows the implementation of 1st-stage DAC_A and the TI residue amplification. The input signal is pre-charged at top-plate of entire array via switch S_s , which is bootstrapped and controlled by Φ_s . Since the TI switches (S_1 and S_2) are kept on until its corresponding conversion is completed, no timing mismatches happen between two channels. During bit cycling, the RAC_{A1} is involved in SA conversion and grounded to scale down the reference voltage [5], while another one RAC_{A2} serves as a flip-around MDAC that feeds back a $16C_0$ to opamp's output for the $4 \times$ residue amplification. The 6b DAC_A is assigned as segment thermometer-code array instead of binary-weighted one to avoid the extra decode logic in SAR controller that reduces the loop delay. The DAC_A and each RAC contain the same total units of $64C_0$ that is determined by the thermal noise. A custom designed unit capacitance of 5.5fF is formed with fringe structure ($2\mu m \times 2.4\mu m$) using the metal layer 1-5. The total input capacitance is

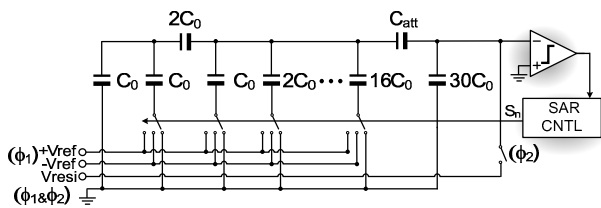


Fig. 3 2nd-stage 6b SAR ADC implementation

1.4pF single-ended, half of which is from DAC_B and RAC_B. The switches S₁ and S₂ implemented between the DAC_A and RAC_A increase RC time constant required for each bit settling, which is relaxed to $\pm 1/2^8 V_{FS}$ due to 1b digital error correction. The small residue swing at the end of the 1st-stage conversion ($< 18.75mV_{p-p}$) allows the switch to be designed with gate capacitance $< 10fF$ (3% of the RAC_A of 350fF), so that the error of charge injection and clock feedthrough is controlled within 10-bit accuracy. The channel gain mismatch mainly due to the mismatches between RAC_{A1} and RAC_{A2} are tolerated within the design constraint. The opamp implemented as a telescopic structure with gain-boosting [5] achieves 1.7GHz GBW and an open-loop gain of 69dB that is sufficient to suppress the opamp's finite gain error and memory effect. The comparators used in 1st- and 2nd-stage SAR are dynamic latch [5] for low power dissipation.

With $\times 4$ inter-stage gain, the 2nd-stage SAR quantizing the residue from the 1st-stage is $1/16V_{in-FS}$. Besides, by 1b overlapping, $\pm V_{ref-2nd}$ is required to be equal to $\pm 1/16V_{ref-1st}$. Thus a 6b DAC with an attenuator C_{att} is used to scale down the reference by 16 as shown in Fig.3. The capacitance of C₀ and C_{att} is 5.5fF and 12fF, respectively. The low total equivalent capacitance of 176fF improves the bandwidth of the opamp.

The top-plate sampling avoids the extra charges transfer of input signal at the bottom to the top-plate of the DAC. Also, the distributed bottom-plate sampling switches is replaced by one top-plate switch S_s that simplifies the layout routing. However, the top-plate sampling together with the mismatch of C_{att} result in an overall inter-stage gain error, which is measured by using the code histogram statistics and calibrated in digital domain by multiplying a gain factor to 5b 2nd-stage digital output. The gain error calibration is implemented off-chip together with the digital error correction logic. In practice, the inter-stage gain error can be calibrated on-chip with low cost, which has already been implemented in our 2nd design. The offsets including the comparators in 1st- and 2nd-stage as well as the opamp are all on-chip calibrated by similar solutions done in [5]. The supplies are used directly as reference voltages for 1st- and 2nd-stage SA conversions.

Measurement Results

The ADC occupies $0.046mm^2$ ($330\mu m \times 140\mu m$) core area and is fabricated in 1P7M 65nm CMOS with low-V_T option. Its die photo is shown in Fig. 4. Fig. 5 presents the measured SNDR of 20 chips. The chip with mean SNDR is selected to report the rest measurement results. Fig.6 shows both the measured FFT @ DC and near Nyquist input. Fig.7 shows the measured dynamic performances with and without gain calibration. The resulting ERBW is 280MHz. The DNL/INL before and after offset and gain calibrations are 22.7/19.5LSB and 0.49/1.1LSB, respectively. The total power consumption

is 8.2mW at a 1.2V supply, including 4.5mW analog power (S/H, DAC, comparators and opamp) and 3.7mW digital power (clock generator, SAR logic and offset calibration). The performance summary and comparison with State-of-the-art ADCs are shown in Table I.

Acknowledgment

The authors would like to thank Si-Seng Wong and Hou-Lon Choi for the measurement support.

References

- [1] T. Miki, et al., "An 11b 300MS/s 0.24pJ/Conversion-Step Double-Sampling Pipelined ADC with On-chip Full Digital Calibration for all nonidealities including Memory Effects," *VLSI Dig. Tech. Papers*, pp. 122-123, Apr. 2011.
- [2] J. Mulder, et al., "An 800MS/s Dual-Residue Pipeline ADC in 40nm CMOS," *ISSCC Dig. Tech. Papers*, pp. 184-185, Feb. 2011.
- [3] A. Verma, B. Razavi, "A 10-Bit 500-MS/s 55-mW CMOS ADC," *IEEE JSSC*, vol.44, NO. 11, pp. 3039-3050, Nov. 2009.
- [4] Y. D. Jeon, et Al., "A 9.15mW 0.22mm² 10b 204MS/s Pipelined SAR ADC in 65nm CMOS" *CICC Dig. Tech. Papers*, pp.1-4, Oct. 2010.
- [5] Y. Zhu, et Al., "A 35 fJ 10b 160 MS/s Pipelined-SAR ADC with Decoupled Flip-Around MDAC and Self-Embedded Offset Cancellation," *A-SSCC Dig. Tech. Papers*, pp.1-4, Nov. 2011.

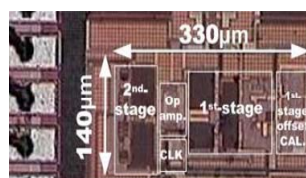


Fig.4 Die chip photograph.

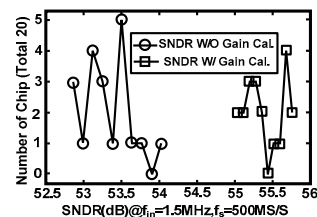


Fig.5 Measured SNDR Histogram.

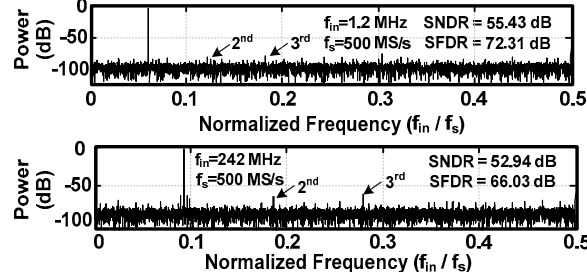


Fig. 6 16384 point FFT for 1.2&242MHz inputs (decimated by 25).

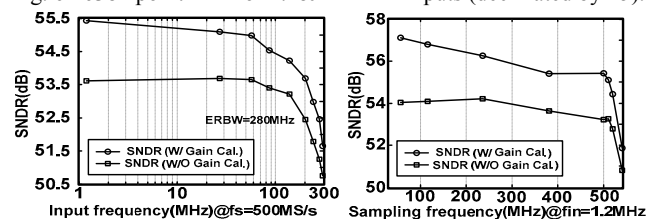


Fig. 7 Dynamic performance of the ADC (w/w/o gain calibration).

TABLE I : Performance Summary and Comparison

	[1]	[2]	[3]	[4]	This Work	
	VLSI' 11	ISSCC' 11	JSSC' 09	CICC' 10	(w/w/o gain cal)	
Architecture	Pipeline	Pipeline	Pipeline	Pipeline-SAR	Pipeline-SAR	
Technology (nm)	40	40	90	65	65	
Resolution (bit)	11	12	10	10	10	
Sampling Rate (MS/s)	300	800	500	204	500	
Supply Voltage (V)	1.8	1/2.5	1.2	1	1.2	
Power (mW)	40	105	55	9.5	8.2	
Area (mm ²)	0.42	0.88	0.5	0.22	0.046	
DNL/INL (LSB)	0.3/1.5	0.4/2.1	0.4/1	0.74/0.9	0.48/1.1	0.58/1.6
SNDR (dB)	56.6	59	52.8	55.2	55.4	53.6
FoM = Power/(2 ^{ENOB@DC} f _s) (fJ/conv.-step)	240	180	310	95.4	34	42